<center>**Supporting Information**</center>

The tricyclic alkaloid catalyzed crystallization of α-FAPbI₃ for high performance antisolvent-free perovskite solar cells

Zhengzhe Wu,‡[a] Haoyu Cai,‡[a] Tong Wu,[a] Jiayi Xu,[a] Zhenyue Wang,[a] Hongqiang Du,[a] Juan Zhao,[b] Fuzhi Huang,[a] Yi-Bing Cheng,[a,c] Jie Zhong [a,]*

[a]State Key Laboratory of Advanced Technology for Materials Synthesis and Processing, Wuhan University of Technology, Wuhan 430070, P. R. China
[b]School of Automobile Engineering, Wuhan University of Technology, Wuhan 430070, P. R. China
[c]Foshan Xianhu Laboratory of the Advanced Energy Science and Technology Guangdong Laboratory, Foshan 528216, Guangdong Province, P. R. China

* E-mail address: jie.zhong@whut.edu.cn

Experimental Section

Materials:

Methylamine hydrochloride (MACl), formamidinium iodide (FAI), FK209, poly[bis (4-phenyl)(2,4,6-trimethylphenyl)amine] (PTAA) and [6,6]-Phenyl-C_{61}-butyric acid methyl ester ($PC_{61}BM$) were purchased from Xi'an Yuri Solar Co., Ltd. Lead iodide (PbI_2) and 4-Isopropyl-4'-methyldiphenyliodonium Tetrakis(pentafluorophenyl)borate (TPFB) was purchased from TCI Chemicals Co., Ltd. Tin (II) chloride dihydrate ($SnCl_2 \cdot 2H_2O$, >99.995%), lithium bis(trifluoromethylsulphonyl)imide (Li-TFSI), 1-cyclohexyl-2-pyrrolidone (CHP, 99%), 4-tert-butylpyridine (tBP), 2-methoxyethanol (2-ME), thioglycolic acid (TGA, 98%), chlorobenzene (CBZ, 99.8%) and acetonitrile (ACN, 99.8%) were purchased from Sigma Aldrich Trading Co., Ltd. 2,2',7,7'-Tetrakis[N,N-di(4-methoxyphenyl)amino]-9,9'-spirobifluorene (Spiro-OMeTAD) was purchased from Shenzhen Feiming Science and Technology Co., Ltd. Urea was purchased from Shanghai Aladdin Biochemical Technology Co., Ltd. Colchicine (Ch) was purchased from Beijing Innochem Science and Technology Co., Ltd. All materials were used as receives without any further purification.

Preparation of perovskite precursor and HTL solution:

The mixed perovskite precursor solution was prepared by dissolving 189.17mg FAI, 567.04mg PbI_2, 33.76mg MACl and 66μL CHP in 1mL 2-ME. The perovskite with Ch was obtained by adding different molar ratios of Ch to achieve 0.01mol%, 0.05mol%, 0.1mol%, 0.5mol%, and 1mol% doped perovskite precursor. The solution was continuously stirred for 30 min before use. The Spiro-OMeTAD solution was prepared by dissolving 73 mg Spiro-OMeTAD into 1 mL chlorobenzene, followed by the addition of 18 μL Li-TFSI (pre-dissolved as a 520 mg mL^{-1} stock solution in acetonitrile) and 29 μL FK209 (pre-dissolved as a 300 mg mL^{-1} stock solution in acetonitrile) and 30 μL 4-tert-butylpyridine. The solution was continuously stirred for 15 min before use. The PTAA solution was prepared by dissolving 30 mg PTAA in 1 mL CBZ (the weight ratio of PTAA/TPFB was 10:1)[1].

Device fabrication:

The FTO substrate was etched by a nanosecond laser machine. Subsequently, the substrate

was cleaned with detergent, followed by ultrasonic cleaning with pure water and 95% ethanol solution for 20 minutes each. Finally, dry the cleaned FTO glass with dry-air gas flow. The compact SnO_2 ETL was deposited by chemical bath deposition (CBD), which was reported in the previous work[2]. Before device fabrication, all the substrates were treated by UV illumination for 15 min. The perovskite films were deposited onto SnO_2 ETL in an N_2 glovebox with 25 µL mixed perovskite solution spin-coating at 5000 rpm for 30 s (an accelerated speed of 1000 rpm), followed by an annealing process at 150 °C and 100°C for 15 min each. After cooling down, 30 µL of Spiro-OMeTAD solution was deposited onto the perovskite layer at 4000 rpm for 20 s with an accelerated speed of 2000 rpm. For the device thermal stability and light stability test, PTAA doped with TPFB was used to replace Spiro-OMeTAD as the hole-transport layer. The PTAA solution was deposited on top of the perovskite layer at a spin rate of 2000 rpm for 30 s[1]. Finally, the Au electrode (80 nm) was deposited by thermal evaporation. For module fabrication, the 5 cm × 5 cm FTO substrate was etched by the nanosecond laser machine to form P1 lines. After the deposition of the Spiro-OMeTAD layer, the module was etched by laser to form P2 lines. Then, the Au electrode was etched by laser to form P3 lines. The final active area of the mini-module is 10.0 cm^2.

Characterizations:

The ^{1}H and ^{13}C-NMR spectra were conducted in DMSO-d6 using a Bruker Avance Neo (400MHz) spectrometer. Fourier transform infrared spectroscopy (FTIR) was measured by the Thermo Scientific Nicolet 6700, with a wavelength range of 4000-400 cm^{-1}. The UV−vis absorption spectra were measured with an ultraviolet spectrometer (Shimadzu UV-1900i), using DMF as the solvent test solution. The samples of perovskite films without and with additives were investigated by an X-ray photoelectron spectroscopy (XPS, ESCALAB 250Xi, Thermo Scientific K-Alpha). The in-situ X-ray diffraction (XRD) patterns were obtained by the D8 Advance in the atmosphere. The spin-coated precursor films were placed on a temperature-controlled stage set to 150°C. The homemade in-situ UV-vis tests were carried out using a QE65 Pro UV−vis spectrometer (Ocean Optics). The illustrated setting is shown in Fig. S17. The sample is spun on a glass with an evaporated Ag substrate. Light from a tungsten light source passes through an optical fiber and a convex lens before illuminating the sample. Light passing through the sample is reflected by the silver on the back of the glass to a convex lens

and finally into the signal collector. Grazing-incidence wide-angle x-ray scattering (GIWAXS) was performed with an incident angle of 0.1° using an Xeuss 3.0 system equipped with an Eiger2R 1M detector. The data of GIWAXS measurements were analyzed by Fit-2D software. The surface morphologies and the cross-sectional SEM images of all samples were attained using field-emission scanning electron microscopy (Hitachi S-4800). The contact angle of all perovskite films using a contact angle tester (Theta Lite, Biolin Scientific). The surface roughness of perovskite films was measured by an atomic force microscope (AFM, Cypher S, Oxford Instruments Asylum Research). Kelvin probe force microscopy (KPFM) was measured by the Cypher S, Oxford Instruments Asylum Research. The ultraviolet photoelectron spectrometer (UPS, Thermo ESCALAB XI+) was tested to estimate the work function and valence band of perovskite films. The steady-state PL and time-resolved PL decay spectrum were measured by a 485 nm picosecond pulsed diode laser (HORIBA Scientific Company, Japan; Nano LED-C2 N-485L). The J-V curves of the perovskite solar cells were measured using a solar simulator (Oriel 94023A, 300 W) and a Keithley 2400 source meter under AM 1.5G illumination intensity with the power density of 100 mW cm^{-2} calibrated by a standard Si solar cell (Oriel VLSI standards). The devices were tested using a metal mask of 0.1475 cm^2 or 1 cm^2 with a scan rate of 10 mV s^{-1}. The Electrical impedance spectroscopy (EIS), Mott-Schottky curves, dark J-V curves, and SCLC were performed by using the electrochemical workstation EC-lab (SP300) in the dark. The External quantum efficiency (EQE) was characterized by a solar cell spectral response measurement system (EnliTechnology Co., Ltd., QE-R). The long-term MPP tracking was carried out on a Multi-Channels Solar Cells Stability Test System from Wuhan 91PVKSolar Technology Co. Ltd, China.

Theoretical calculation:

In this paper, the geometry optimization and Mulliken charge distribution were performed using the density functional theory (DFT) calculation[3]. The hybrid B3LYP-D3 exchange-correlation functional was used to investigate geometrical transformations and interactions in the Ch and precursor perovskite systems. The interaction energy was calculated using the equation: $E_{int} = E_{ab} - E_a - E_b + E_{BSSE}$, where E_{ab}, E_a, and E_b are thermo-corrected energies of the adduct and two components, E_{BSSE} the basis set superposition error correction term. The C, H, O, and N in Ch and precursor perovskite molecules were calculated with the jul-cc-pvtz basis set, while Pb and I were treated by lanl08(d) and visualized by VMD[4].
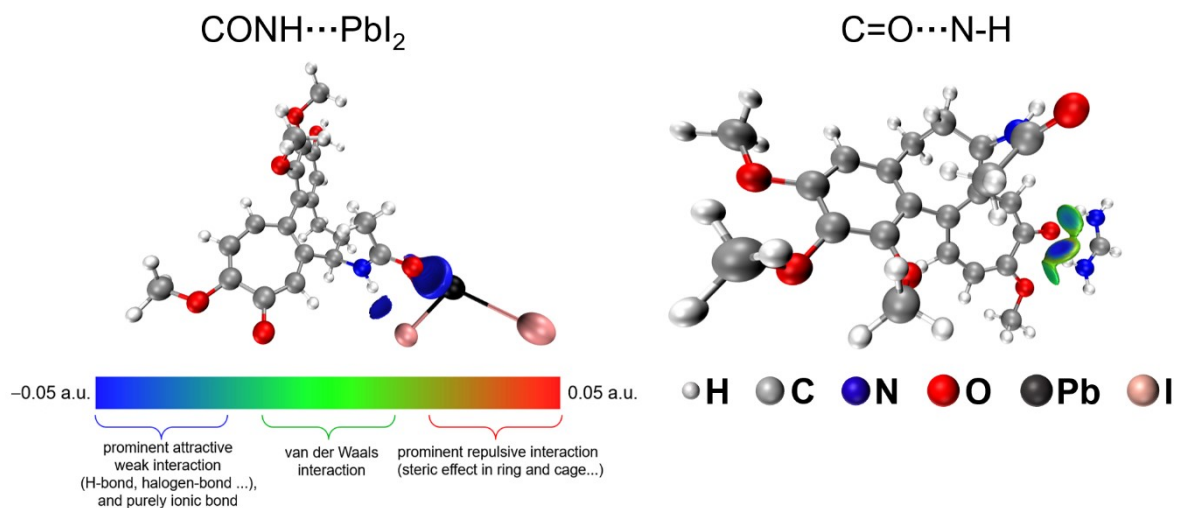
CONH···PbI$_2$ C=O···N-H

−0.05 a.u.   0.05 a.u.

prominent attractive weak interaction (H-bond, halogen-bond ...), and purely ionic bond

van der Waals interaction

prominent repulsive interaction (steric effect in ring and cage...)

○H ○C ●N ●O ●Pb ○I

Fig. S1 Visualization of weak interactions between Ch and PbI$_2$/FAI.
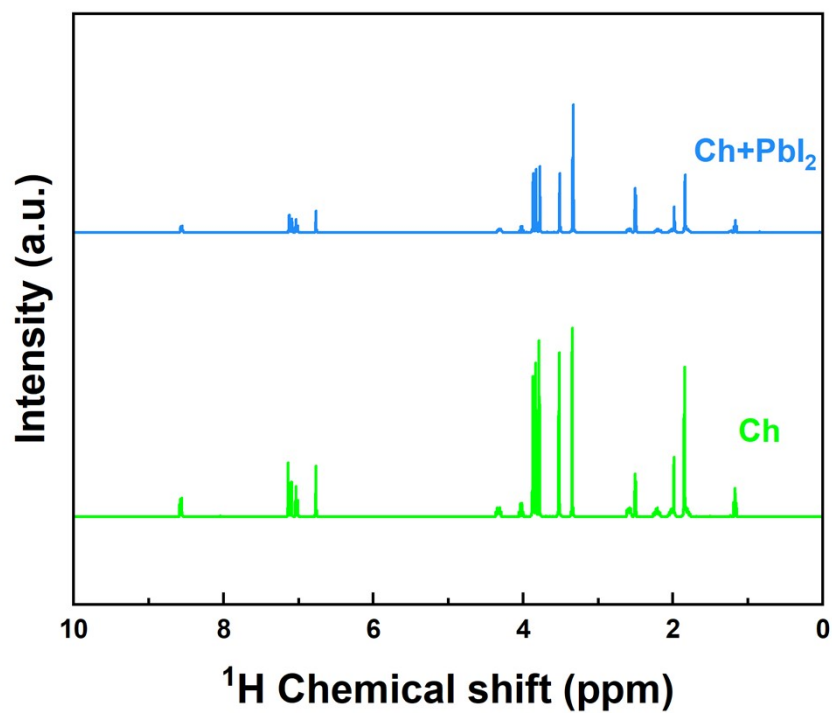
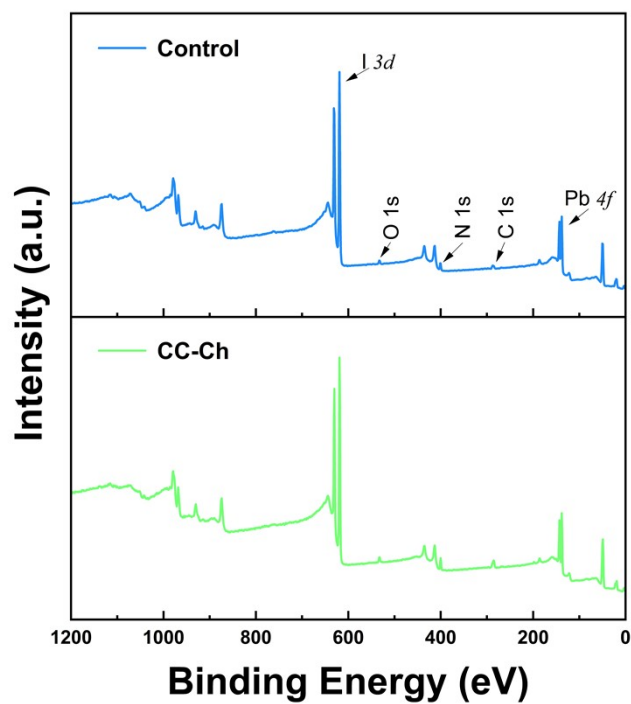**Fig. S2** A comparison of ^{1}H NMR spectra of Ch and Ch+PbI$_2$.

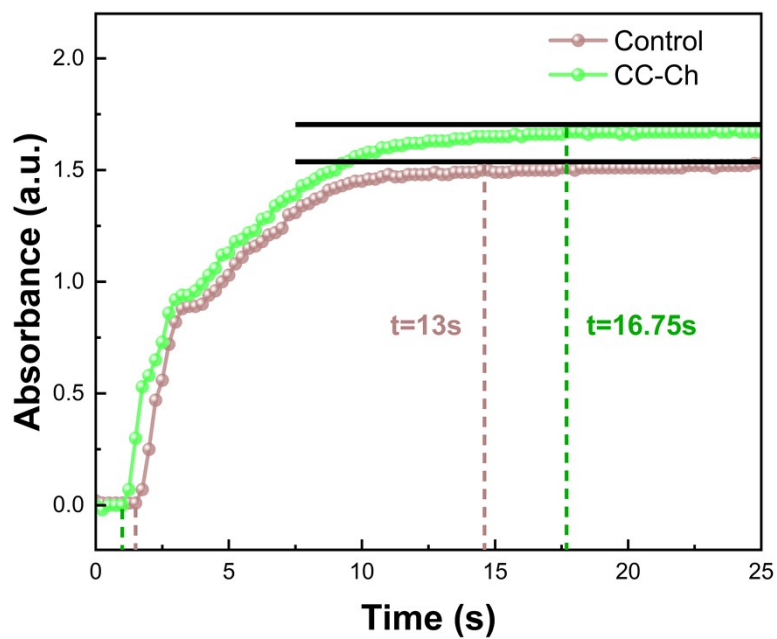**Fig. S3** The full XPS spectra of perovskite films without and with Ch additive.

Fig. S4 Dynamical evolution of absorption intensity at 750 nm for perovskite films without and with Ch additive during thermal annealing.
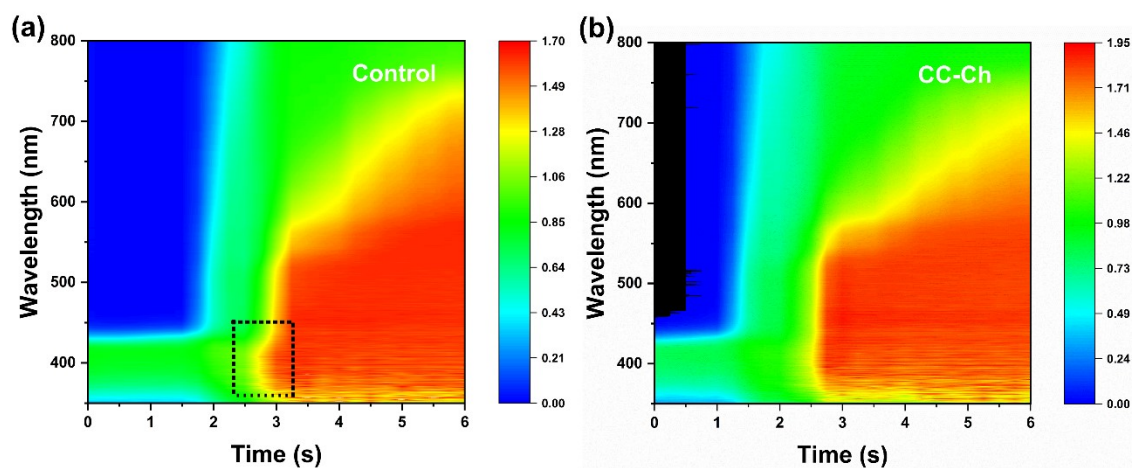
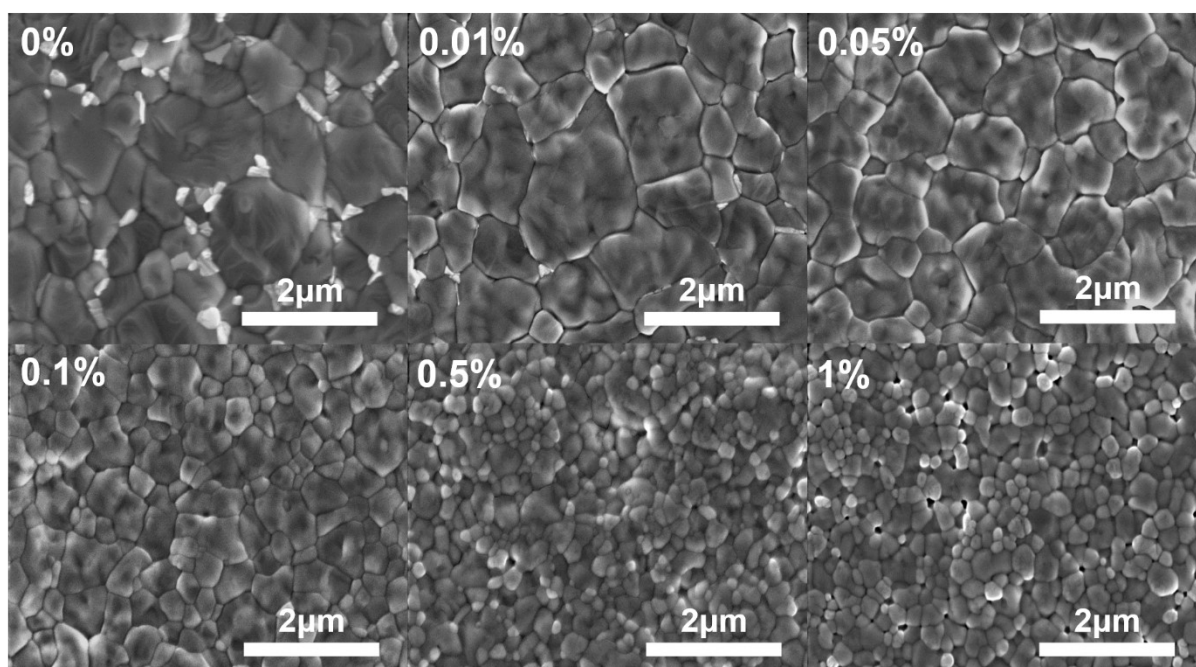**Fig. S5** In-situ UV-vis absorption spectra during the initial annealing process: a) Control and b) CC-Ch.

Fig. S6 The surface morphologies SEM images of perovskite films with different concentrations of Ch additives.
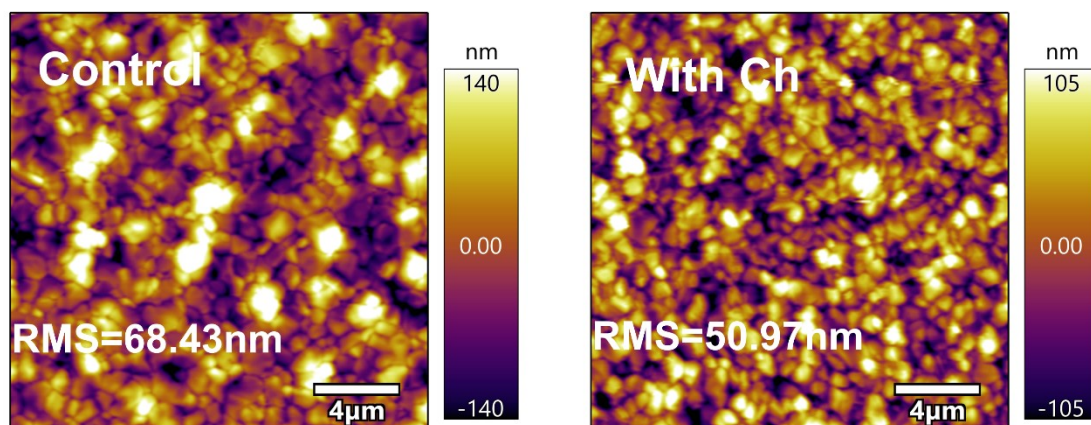
Fig. S7 The AFM topography images of perovskite films without and with Ch additive, the graph size is 20 × 20 μm.
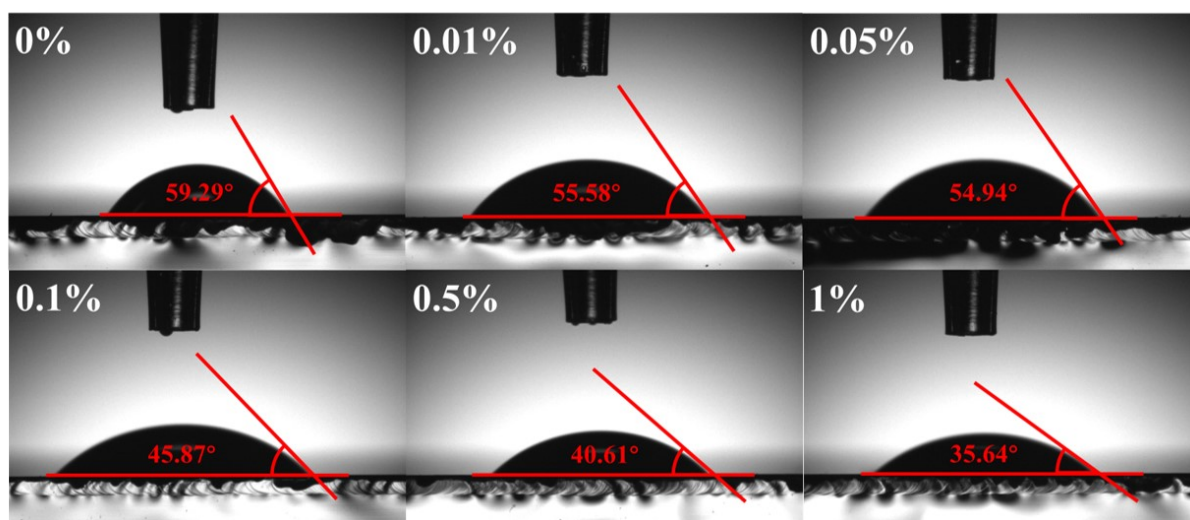

Fig. S8 The contact angle measurements of perovskite films with different concentrations of Ch additives.
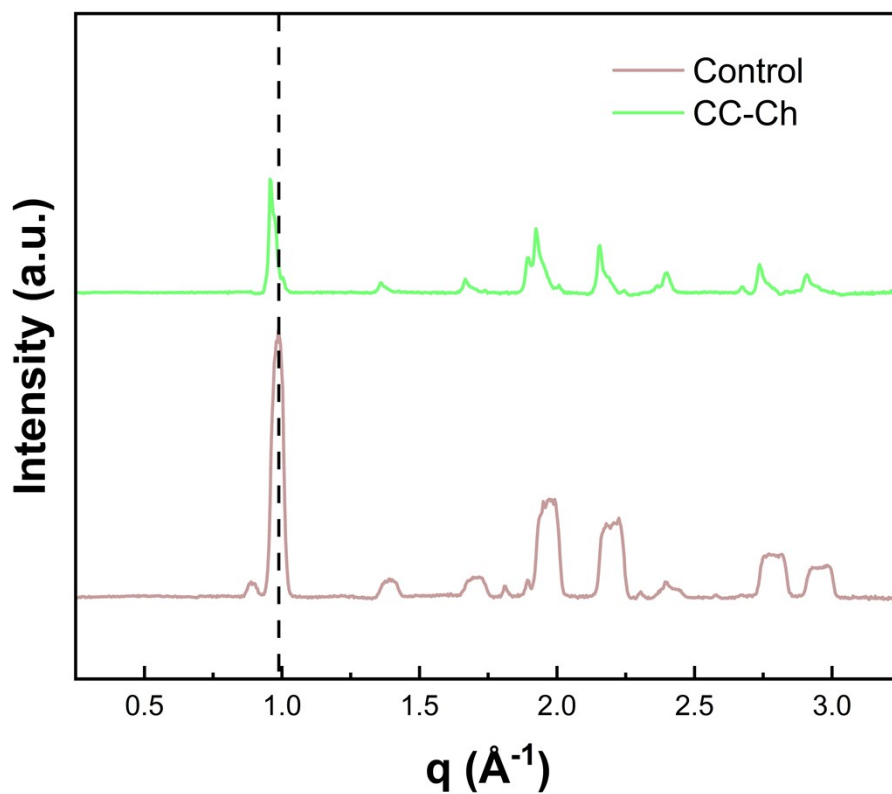
Fig. S9 1D GIWAXS patterns of perovskite films without and with Ch additive.
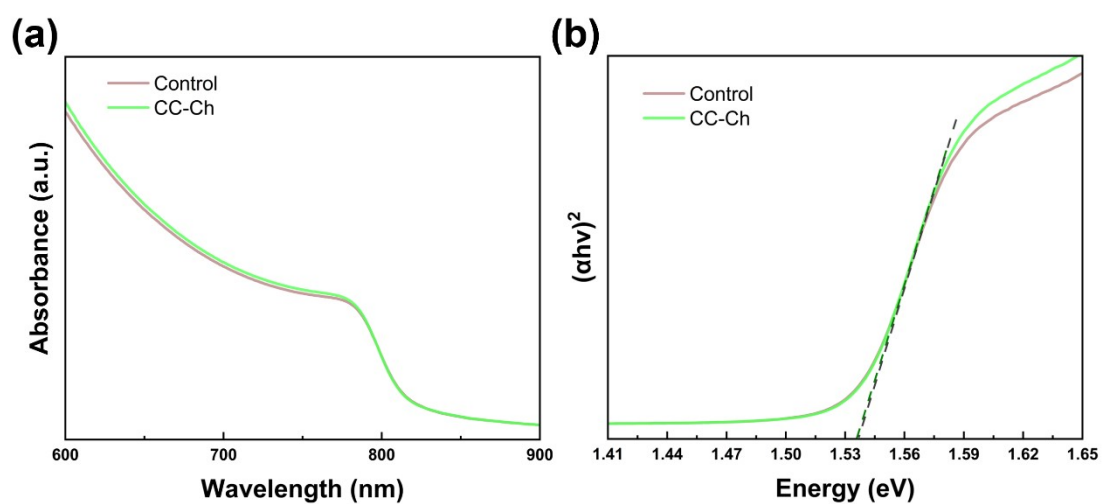
Fig. S10 (a) UV-vis absorption spectra of the Control and CC-Ch perovskite films. (b) Tauc-plot of the Control and CC-Ch perovskite films.
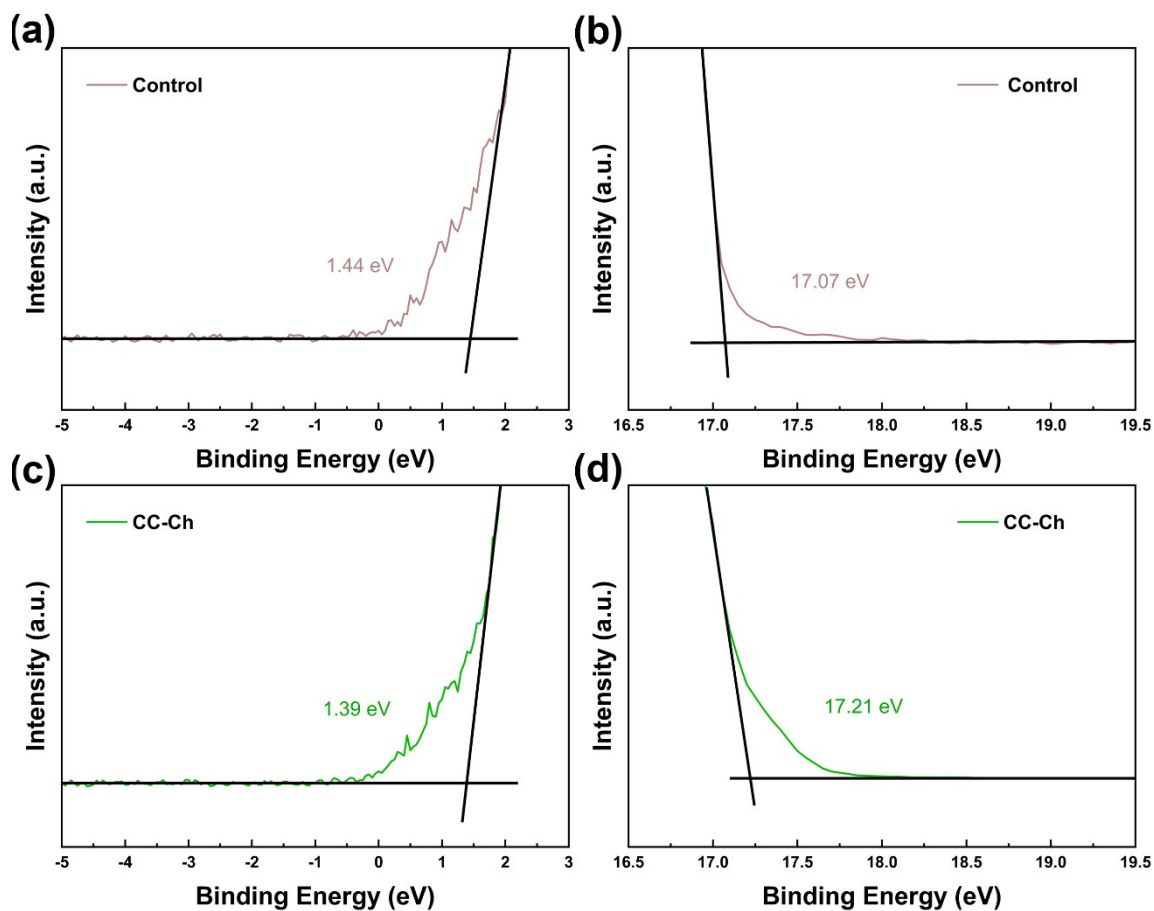
Fig. S11 UPS spectra: $E_{F\text{-edge}}$ of (a) Control and (c) CC-Ch perovskite films. $E_{cut\text{-off}}$ of (b) Control and (d) CC-Ch perovskite films.
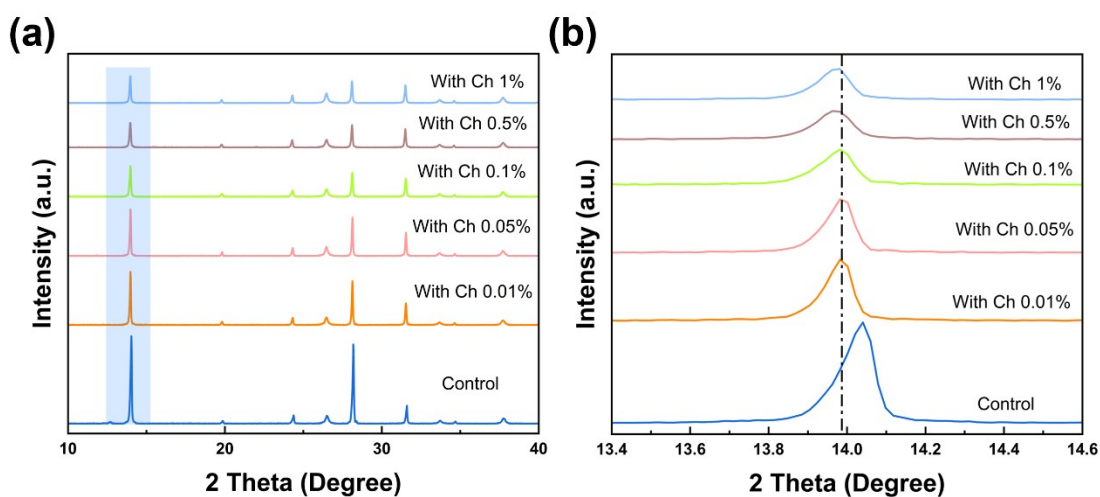
Fig. S12 (a) XRD spectra of perovskite films with different concentrations of Ch additives. (b) XRD spectra in the (100) plane position from (a).
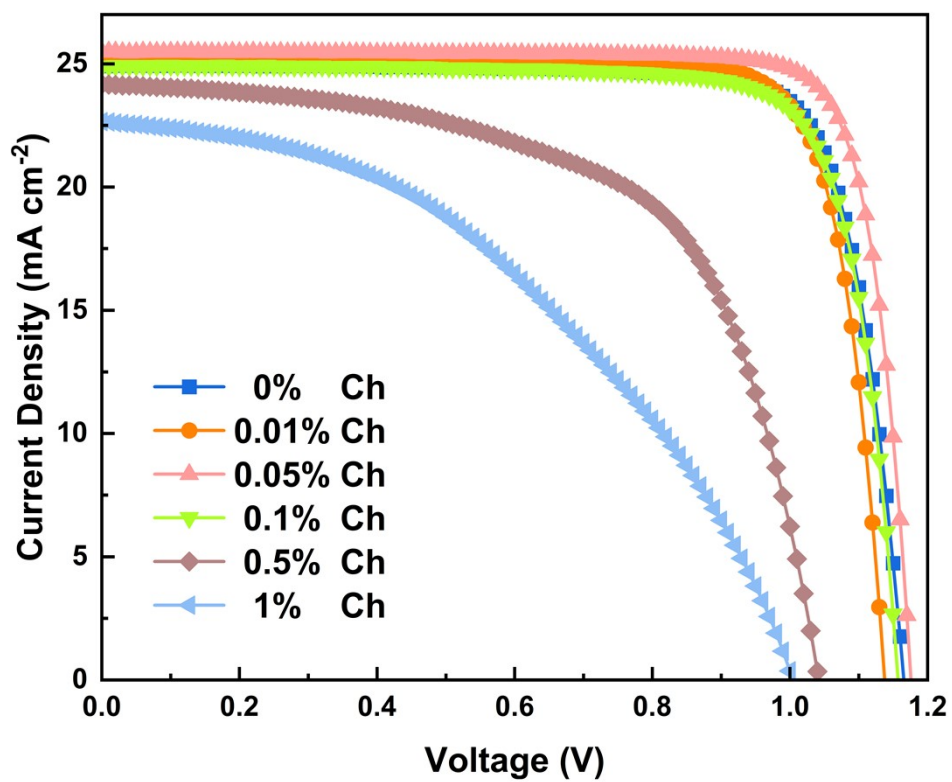
Fig. S13 Current density–voltage curves for champion devices incorporating different concentrations of Ch additives.
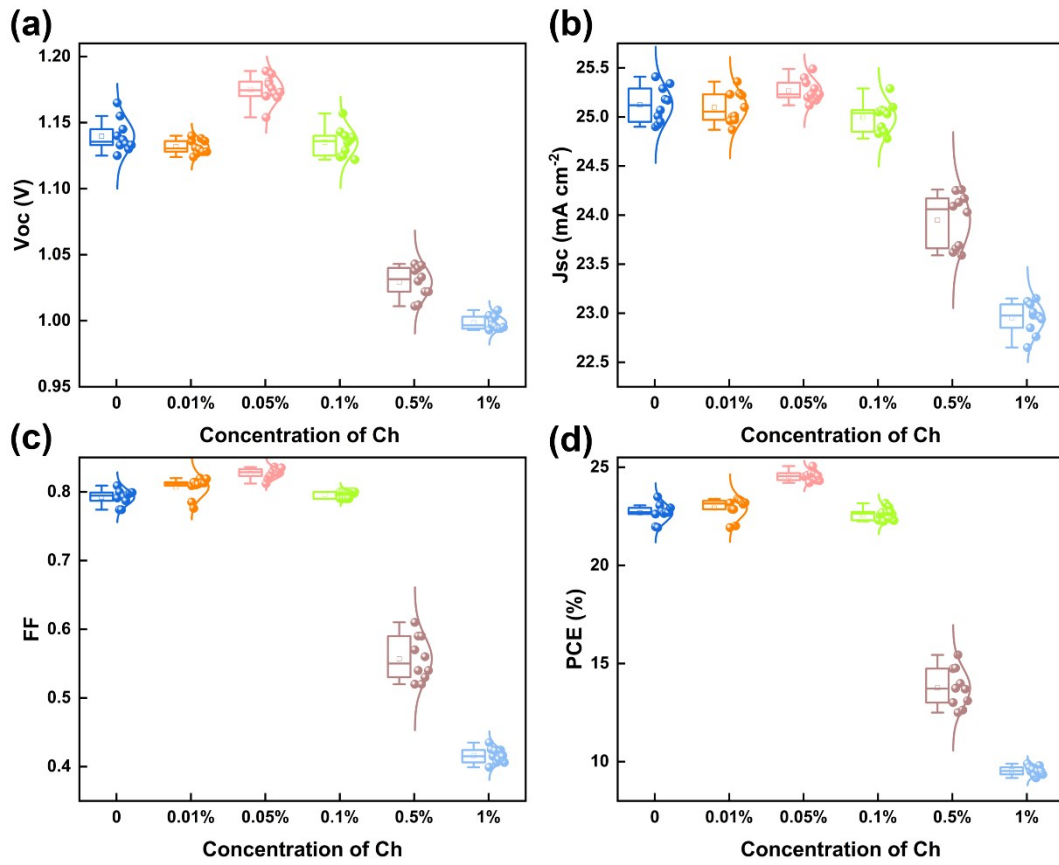
Fig. S14 Photovoltaic parameters statistics of a) V_{OC}, b) J_{SC}, c) FF, and d) PCE based on 10 devices with different concentrations of Ch additives.

	Voc(V)	Jsc (mA cm^{-2})	FF	PCE(%)
Control	1.152	24.96	0.668	19.20
CC-Ch	1.187	24.92	0.730	21.58
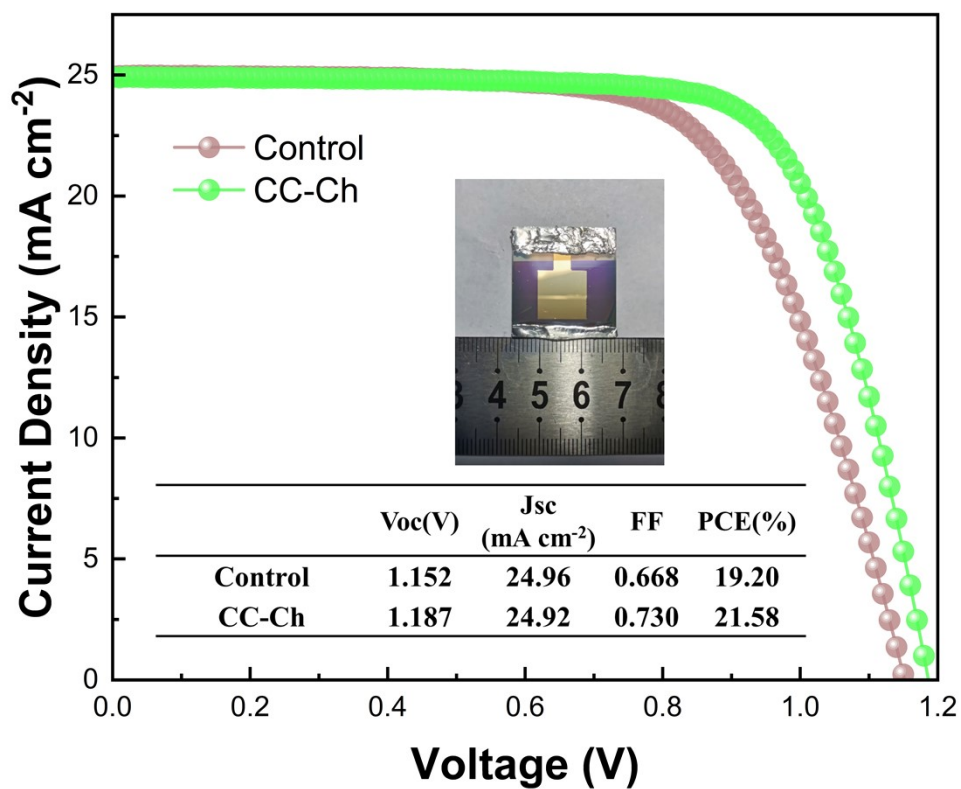
Fig. S15 *J-V* curves of the large area (aperture area: 1 cm^2) PSCs with and without Ch additive. The insert figure is a photograph of the large area of PSCs.

	Voc(V)	Jsc (mA cm^{-2})	FF	PCE(%)
Control	6.428	3.95	0.615	15.61
CC-Ch	6.781	3.95	0.750	20.08
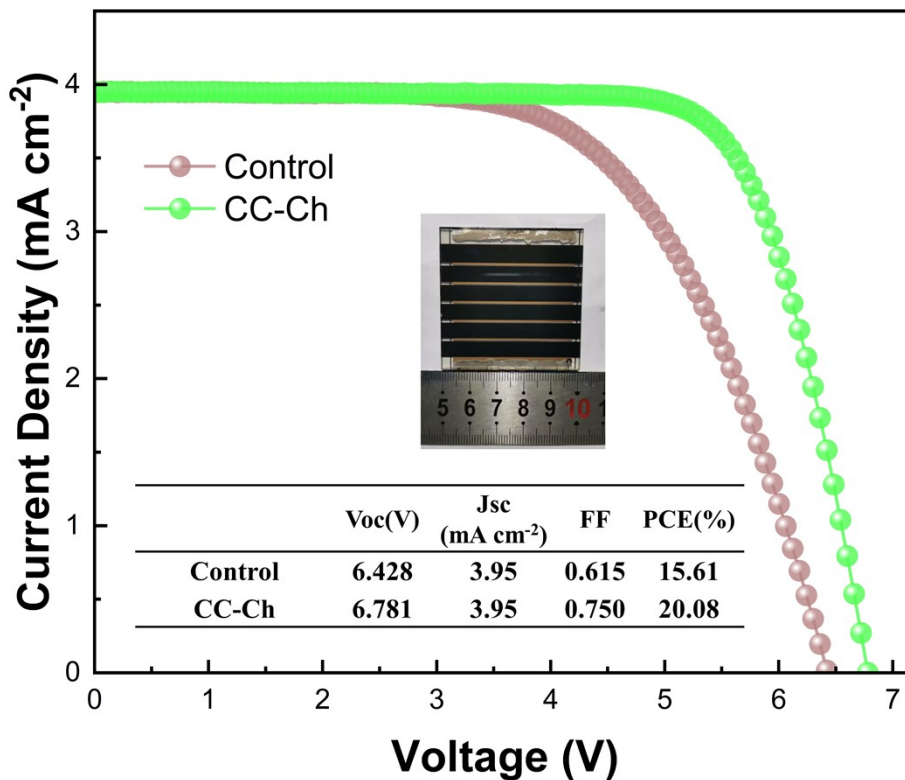
Fig. S16 *J-V* curves of the perovskite solar mini-modules (aperture area: 10 cm^2) with and without Ch additive. The insert figure is a photograph of the perovskite solar mini-modules.
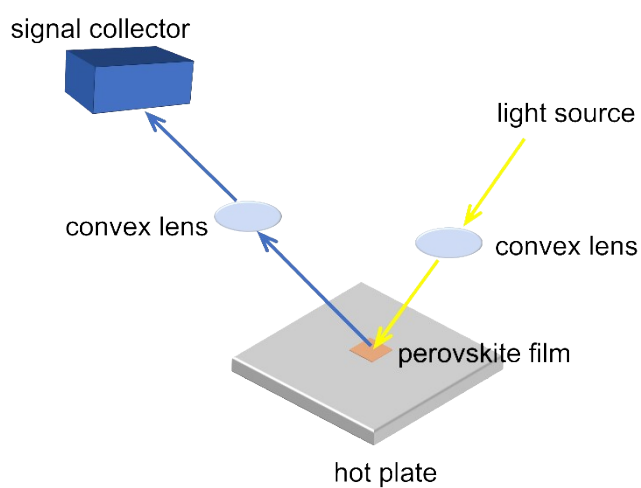
Fig. S17 Schematic picture of the in-situ UV-vis absorption measurement consisting of the light source, convex lens, hot plate, and signal collector.

Table S1 Calculated parameters of the band structure for perovskite films without and with Ch additive.

| Sample	$E_{cut\text{-}off}$ (eV)	W_F (eV)	$E_{F\text{-}edge}$ (eV)	E_{VB} (eV)	E_g (eV)	E_{CB} (eV)
Control	17.07	-4.15	1.44	-5.59	1.54	-4.05
With Ch	17.21	-4.01	1.39	-5.40	1.54	-3.86

Table S2 The position and FWHM of XRD in the (100) plane of the Control and With Ch perovskite films.

Sample	Position (degree)	FWHM (degree)
Control	14.04	0.102
With Ch	13.98	0.091

Table S3 Fitting parameters of the TRPL spectra for perovskite films without and with Ch additive.

Sample	τ_{ave} (ns)	τ_1 (ns)	τ_2 (ns)	A_1	A_2
Control	605.08	190.82	704.85	0.532	0.598
With Ch	1982.40	743.39	2141.51	0.246	0.665

Table S4 Calculated parameters and trap density (n_t) of perovskite films without and with Ch additive.

Sample	L (nm)	V_{TFL} (V)	n_t (cm^{-3})
Control	600	0.15	2.162×10^{15}
With Ch	600	0.11	1.585×10^{15}

Table S5 EIS fitting parameters for perovskite films without and with Ch additive.

Sample	R_s(Ohm)	R_{ct}(Ohm)	C_{ct}(F)
Control	12.52	5714	1.764×10^{-8}
With Ch	10.16	2678	2.086×10^{-11}

Table S6 Performance comparison of devices dominated by $FAPbI_3$ perovskite components.

Perovskite system	Solvent	Methods	Device area	PCE	Years
$FAPbI_3$	DMF+NMP	Antisolvent-free	0.121 cm^2	19.4%	2021[5]
$FAPbI_3$	2-ME+NMP	Antisolvent-free		20.1%	2022[6]
$FAPbI_3$	EtOH+DMA	Antisolvent-free	0.094 cm^2	25.1%	2022[7]
$FAPbI_3$	DMF	Antisolvent-free	0.05 cm^2	23.91%	2022[8]
$Cs_{0.1}FA_{0.9}PbI_3$	DMF+NMP	Antisolvent-free	0.09 cm^2	23.27%	2022[9]
$FAPbI_3$	DMF	Antisolvent-free	0.05 cm^2	23.15%	2023[10]
$FAPbI_3$	2-ME	Antisolvent-free		23.6%	2024[11]
$FAPbI_3$	ACN+DMF+DMSO	Blade coating	0.062 cm^2	24.32%	2023[12]

Perovskite system	Solvent	Methods	Device area	PCE	Years
$FAPbI_3$	2-ME	Bar coating	0.094 cm^2	24.53%	2023[13]
$FAPbI_3$	2-ME+ACN+NMP	Slot-die coating	0.096 cm^2	22.54%	2023[14]
$Cs_{0.05}FA_{0.95}PbI_{2.5}Br_{0.05}$	DMF+DMSO+2MeTHF	Blade coating	0.09 cm^2	24.00%	2023[15]
$FAPbI_3$	DMF+DMSO	Antisolvent		25.2%	2023[16]
$FAPbI_3$	DMF+DMSO	Antisolvent	0.073 cm^2	25.41%	2023[17]
$FAPbI_3$	DMF+DMSO	Antisolvent	0.064 cm^2	24.76%	2023[18]
$FAPbI_3$	DMF+DMSO	Antisolvent	0.0755 cm^2	25.4%	2023[19]
$FAPbI_3$	DMF+DMSO	Antisolvent	0.0804 cm^2	24.02%	2019[20]
$FAPbI_3$	DMF+DMSO	Antisolvent	0.08 cm^2	25.7%	2022[21]
$FAPbI_3$	DMF+DMSO	Antisolvent	0.13 cm^2	22.7%	2020[22]
$FAPbI_3$	DMF+DMSO	Antisolvent	0.1 cm^2	23.21%	2022[23]
$FAPbI_3$	DMF+DMSO	Antisolvent	0.096 cm^2	26.08% (certified 25.73%)	2023[24]
$FAPbI_3$	DMF+DMSO	Antisolvent	0.095 cm^2	24.9%	2022[25]
$FAPbI_3$	DMF+DMSO	Antisolvent	0.08 cm^2	25.35%	2024[26]
$FAPbI_3$	DMF+DMSO	Antisolvent	0.0805 cm^2	25.6% (certified 25.2%)	2021[27]
$FA_{0.98}Cs_{0.02}PbI_3$	DMF+NMP+DBSO	Antisolvent	0.0897 cm^2	25.1%	2023[28]
$(FAPbI_3)_{0.95}(MAPbBr_3)_{0.05}$	DMF+DMSO	Antisolvent		22.39%	2021[29]
$FAPbI_3$	DMF+NMP	Antisolvent		21.6%	2021[30]
$FAPbI_3$	**2-ME**	**Antisolvent-free**	**0.1475 cm^2**	**25.06%**	**Our work**

References

1. Y. Zhao, F. Ma, Z. Qu, S. Yu, T. Shen, H.-X. Deng, X. Chu, X. Peng, Y. Yuan, X. Zhang and J. You, *Science*, 2022, **377**, 531-534.

2. J. B. Zhang, C. Bai, Y. Dong, W. J. Shen, Q. Zhang, F. Z. Huang, Y. B. Cheng and J. Zhong, *Chem. Eng. J.*, 2021, **425**, 131444-131452.

3. M. J. Frisch, G. W. Trucks, H. B. Schlegel, G. E. Scuseria, M. A. Robb, J. R. Cheeseman, G. Scalmani, V. Barone, G. A. Petersson, H. Nakatsuji, X. Li, M. Caricato, A. V. Marenich, J. Bloino, B. G. Janesko, R. Gomperts, B. Mennucci, H. P. Hratchian, J. V. Ortiz, A. F. Izmaylov, J. L. Sonnenberg, Williams, F. Ding, F. Lipparini, F. Egidi, J. Goings, B. Peng, A. Petrone, T. Henderson, D. Ranasinghe, V. G. Zakrzewski, J. Gao, N. Rega, G. Zheng, W. Liang, M. Hada, M. Ehara, K. Toyota, R. Fukuda, J. Hasegawa, M. Ishida, T. Nakajima, Y. Honda, O. Kitao, H. Nakai, T. Vreven, K. Throssell, J. A. Montgomery Jr., J. E. Peralta, F. Ogliaro, M. J. Bearpark, J. J. Heyd, E. N. Brothers, K. N. Kudin, V. N. Staroverov, T. A. Keith, R. Kobayashi, J. Normand, K. Raghavachari, A. P. Rendell, J. C. Burant, S. S. Iyengar, J. Tomasi, M. Cossi, J. M. Millam, M. Klene, C. Adamo, R. Cammi, J. W. Ochterski, R. L. Martin, K. Morokuma, O. Farkas, J. B. Foresman and D. J. Fox, *Journal*, 2016.

4. T. Lu and Q. Chen, *J. Comput. Chem.*, 2022, **43**, 539-555.

5. K. M. M. Salim, S. Masi, A. F. Gualdrón-Reyes, R. S. Sánchez, E. M. Barea, M. Krečmarová, J. F. Sánchez-Royo and I. Mora-Seró, *ACS Energy Lett.*, 2021, **6**, 3511-3521.

6. Q. Zhang, G. Ma, K. A. Green, K. Gollinger, J. Moore, T. Demeritte, P. C. Ray, G. A. Hill, Jr., X. Gu, S. E. Morgan, M. Feng, S. Banerjee and Q. Dai, *ACS Appl. Energy Mater.*, 2022, **5**, 1487-1495.

7. H.-S. Yun, H. W. Kwon, M. J. Paik, S. Hong, J. Kim, E. Noh, J. Park, Y. Lee and S. Il Seok, *Nat. Energy.*, 2022, **7**, 828-834.

8. L. Chao, Y. Xia, X. Duan, Y. Wang, C. Ran, T. Niu, L. Gu, D. Li, J. Hu, X. Gao, J. Zhang and Y. Chen, *Joule*, 2022, **6**, 2203-2217.

9. D. Wang, J. Chen, P. Zhu, Y. Qiao, H. Hu, J. Zeng, J. Zhang, G. Qu, Y. Wang, X. Wang, A. K.-Y. Jen and B. Xu, *Adv. Energy Mater.*, 2023, **13**, 2203649.

10. T. Niu, L. Chao, Y. Xia, K. Wang, X. Ran, X. Huang, C. Chen, J. Wang, D. Li, Z. Su, Z. Hu, X. Gao, J. Zhang and Y. Chen, *Adv. Mater.*, 2023, 2309171.

11. X. Wu, Y. Zheng, J. Liang, C. Tian, A. Sun, C. Tang, Y. Liu, S. Zhang, C. Wang, S. Song, C.-C. Chen and K. M. Reddy, *Adv. Energy Mater.*, 2024, 2304302.

12. L. Yuan, X. Chen, X. Guo, S. Huang, X. Wu, Y. Shen, H. Gu, Y. Chen, G. Zeng, H.-J. Egelhaaf, C. J. Brabec, F. Yang, Y. Li and Y. Li, *Angew. Chem. Int. Edit.*, 2024, **63**, e202316954.

13. J. W. Yoo, E. Noh, J. Jang, K. S. Lee, J. Byeon, M. Choi, J. Im and S. I. Seok, *Joule*, 2023, **7**, 797-809.

14. J. Li, J. Dagar, O. Shargaieva, O. Maus, M. Remec, Q. Emery, M. Khenkin, C. Ulbrich, F. Akhundova, J. A. Márquez, T. Unold, M. Fenske, C. Schultz, B. Stegemann, A. Al-Ashouri, S. Albrecht, A. T. Esteves, L. Korte, H. Köbler, A. Abate, D. M. Többens, I. Zizak, E. J. W. List-Kratochvil, R. Schlatmann and E. Unger, *Adv. Energy Mater.*, 2023, **13**, 2203898.

15. Y. Du, Q. Tian, S. Wang, L. Yin, C. Ma, Z. Wang, L. Lang, Y. Yang, K. Zhao and S. Liu, *Adv. Mater.*, 2023, 2307583.

16. R. Tian, C. Liu, Y. Meng, Y. Wang, R. Cao, B. Tang, D. Walsh, H. Do, H. Wu, K. Wang, K. Sun, S. Yang, J. Zhu, X. Li and Z. Ge, *Adv. Mater.*, 2023, 2309998.

17. Y. Hu, Q. Zhong, B. Song, H. Xu, Q. Li, S. Li, Y. Qiu, X. Yang, J. Chen, Q. Zhang, R. Zhu and M. Cao, *Angew. Chem. Int. Edit.*, 2024, **63**, e202316154.

18. R. Wang, X. Li, J. Qi, C. Su, J. Yang, S. Yang, M. Yuan and T. He, *Adv. Mater.*, 2023, **35**, 2304149.

19. Y. Meng, Y. Wang, C. Liu, P. Yan, K. Sun, Y. Wang, R. Tian, R. Cao, J. Zhu, H. Do, J. Lu and Z. Ge, *Adv. Mater.*, 2024, **36**, 2309208.

20. M. Kim, G.-H. Kim, T. K. Lee, I. W. Choi, H. W. Choi, Y. Jo, Y. J. Yoon, J. W. Kim, J. Lee, D. Huh, H. Lee, S. K. Kwak, J. Y. Kim and D. S. Kim, *Joule*, 2019, **3**, 2179-2192.

21. M. Kim, J. Jeong, H. Lu, T. K. Lee, F. T. Eickemeyer, Y. Liu, I. W. Choi, S. J. Choi, Y. Jo, H.-B. Kim, S.-I. Mo, Y.-K. Kim, H. Lee, N. G. An, S. Cho, W. R. Tress, S. M. Zakeeruddin, A. Hagfeldt, J. Y. Kim, M. Grätzel and D. S. Kim, *Science*, 2022, **375**, 302-306.

22. Y. Liu, S. Akin, A. Hinderhofer, F. T. Eickemeyer, H. Zhu, J.-Y. Seo, J. Zhang, F. Schreiber, H. Zhang, S. M. Zakeeruddin, A. Hagfeldt, M. I. Dar and M. Grätzel, *Angew. Chem. Int. Edit.*, 2020, **59**, 15688-15694.

23. J. Wang, H. Ma, A. Wang, Z. Li, J. Dong, Y. Liu, S. Gao, S. Yan, X. Chen, Y. Li, Z. Wu, W. Xu, F. Liu, F. Wang, W. Huang and T. Qin, *Matter*, 2022, **5**, 2209-2224.

24. J. Park, J. Kim, H.-S. Yun, M. J. Paik, E. Noh, H. J. Mun, M. G. Kim, T. J. Shin and S. I. Seok, *Nature*, 2023, **616**, 724-730.

25. H. Min, S.-G. Ji and S. I. Seok, *Joule*, 2022, **6**, 2175-2185.

26. H. Zhang, S. Zhang, X. Ji, J. He, H. Guo, S. Wang, W. Wu, W.-H. Zhu and Y. Wu, *Angew. Chem. Int. Edit.*, 2024, e202401260.

27. J. Jeong, M. Kim, J. Seo, H. Lu, P. Ahlawat, A. Mishra, Y. Yang, M. A. Hope, F. T. Eickemeyer, M. Kim, Y. J. Yoon, I. W. Choi, B. P. Darwich, S. J. Choi, Y. Jo, J. H. Lee, B. Walker, S. M. Zakeeruddin, L. Emsley, U. Rothlisberger, A. Hagfeldt, D. S. Kim, M. Grätzel and J. Y. Kim, *Nature*, 2021, **592**, 381-385.

28. R. Chen, J. Wang, Z. Liu, F. Ren, S. Liu, J. Zhou, H. Wang, X. Meng, Z. Zhang, X. Guan, W. Liang, P. A. Troshin, Y. Qi, L. Han and W. Chen, *Nat. Energy.*, 2023, **8**, 839-849.

29. H. Zhang, Z. Chen, M. Qin, Z. Ren, K. Liu, J. Huang, D. Shen, Z. Wu, Y. Zhang, J. Hao, C.-s. Lee, X. Lu, Z. Zheng, W. Yu and G. Li, *Adv. Mater.*, 2021, **33**, 2008487.

30. M. Wang, Y. Yin, W. Cai, J. Liu, Y. Han, Y. Feng, Q. Dong, Y. Wang, J. Bian and Y. Shi, *Adv. Funct. Mater.*, 2022, **32**, 2108567.